

On the Relationship Between the Spatial Correlation of Point Rain Rate and of Rain Attenuation on Earth-Space Radio Links

L. Luini and C. Capsoni

Abstract—This contribution presents an analytical expression to predict the spatial correlation of the rain attenuation A impairing two Earth-space radio links in a site diversity configuration (ρ_A) as a function of the spatial correlation of the rain precipitation affecting the area (ρ_R), of the distance between the two stations d and of the electrical and geometrical characteristics of the links. Well-established properties of the rain field (i.e. quasi-ergodicity and spatial stationarity) are exploited in the derivation of the proposed analytical expression, whose accuracy is evaluated by means of an extensive set of rain field data collected by the NIMROD weather radar network in the UK. Results indicate a satisfactory prediction performance in the 10-50 GHz frequency range, with negligible dependence on the site separation distance d and on the electrical and geometrical characteristics of the system.

Index Terms—Spatial correlation, rain attenuation, radio propagation, satellite systems.

I. INTRODUCTION

FAST and reliable communication systems are an essential need in a world where information transmission is always more important. While cabled networks still represent the largest portion of such systems, wireless technologies are emerging more and more because they can be deployed with a limited effort and offer a large coverage area. Since the seventies, the operational frequency of wireless systems has been continuously increasing in order to face the progressive congestion of lower bands and the need of an always growing data rate (i.e. bandwidth) necessary to provide advanced services. This is the case of modern satellite communication systems, which are nowadays starting to operate in the Ka-band (i.e. above 20 GHz) to offer, as an example, full-duplex Internet connectivity [1]. Unfortunately, the atmosphere is not transparent to radio waves: at frequencies higher than approximately 10 GHz, rain, clouds and gases are the main impairments to be faced by wireless communication systems [2]. Among them, rain has the most severe impact on the system, as the absorption and scattering of electromagnetic

energy due to hydrometeors concur to produce extremely high attenuation of the transmitted signal, which can sometimes even cause the outage of the system [3].

A key feature of rain attenuation, especially when it is associated to very intense precipitation events, is its uneven distribution in time and space [4]. Accurate knowledge of the spatial correlation of the rain attenuation is therefore of great interest in the design of wireless communication systems. In fact, the effectiveness of resource sharing techniques is tightly linked to the probability that two or more stations simultaneously require additional resources to counteract the signal degradation deriving from propagation impairments [5]. Considering the prevalent impact of rain, this probability is strongly dependent on the spatial distribution of the rain attenuation. In site diversity systems, information on the spatial correlation of the rain attenuation as a function of the distance between two or more locations is essential for the proper design of diversity schemes, whose performance improves as the attenuation simultaneously affecting the sites becomes more and more decorrelated [6]. Knowledge of the correlation coefficient is useful also for time series generators and models to be employed in the simulation of satellite networks, where the proper degree of spatial correlation must be maintained in order to generate reliable results [7],[8].

Accurate knowledge of the spatial distribution of rain attenuation can be obtained from time series collected by satellite beacon receivers, which, however, are typically deployed for experimental purpose in a very limited number of sites [9]; moreover, the removal of the signature of clouds and gases from the total measured attenuation is not a trivial task. Rain field data derived from meteorological radars represent a valuable alternative because they allow to estimate the spatial correlation of rain attenuation on a relatively large area (typically in the order of 200 km \times 200 km) for a given set of geometrical (elevation, rainy path length, orientation) and electrical (frequency, polarization) parameters of the link [10]. Unfortunately, such kind of data are not widely available worldwide and not always with the spatial resolution (nor accuracy) necessary to properly sample the rainfall process (typically 1 km \times 1 km).

This contribution presents an analytical relationship between the spatial correlation of the point rain rate (ρ_R) and of the associated attenuation affecting two Earth-space radio links in a site diversity configuration (ρ_A), as a function of the

Manuscript received XX.

Lorenzo Luini and Carlo Capsoni are with the Dipartimento di Elettronica, Informazione e Bioingegneria, Politecnico di Milano, Piazza Leonardo da Vinci, 35, 20133, Milano, Italy (e-mail: lorenzo.luini@polimi.it).

distance between the two stations and of some link characteristics, i.e. frequency and rainy path length. As a result, ρ_A can be simply and directly derived from the knowledge of ρ_R , which, in turn, can be obtained from instruments that are far less expensive and more widely available than beacon receivers or weather radars (e.g. networks of rain gauges or disdrometers [11]).

The remainder of the paper is organized as follows. Based on the quasi-ergodicity and stationarity properties of the rainfall process, the relationship between ρ_A and ρ_R is derived in section II, where the spatial correlation of the rain rate integrated along the path is first addressed as an intermediate step. Section III firstly describes an extensive database of rain fields, collected by a set of weather radars in the UK (NIMROD network), which is used in this work to investigate some properties of the rain field, as well as to derive ρ_R and ρ_A , the latter as a function of the operational frequency f and of the path length L affected by rain. Afterwards, section III evaluates the accuracy of the analytical relationship derived in section II by discussing in detail its dependence on several factors such as L , f . Finally, section IV draws some conclusions.

II. SPATIAL CORRELATION INDEX OF RAIN ATTENUATION

In this work, we will make reference to two radio links, with parallel paths of length L impaired by rain and whose transceivers are set d -km apart (see Fig. 1). This is the typical configuration of two Earth-space links pointing to the same satellite in a site diversity configuration aimed at increasing the overall system performance [6]. In this geometry, L depends on the local rain height h_R and on the elevation angle θ of the links, according to the simple expression $L = h_R/\sin(\theta)$, which assumes invariance of the rain rate with height [12]. For simplicity, but with no lack of generality, we will suppose that those links lie in the North-South direction (the black cell in Fig. 1 represents the position of the station transceiver) and that their path is discretized into N pixels (of negligible height and of width d_{pix} such that $L = N \cdot d_{pix}$), each of which is associated to a constant rain rate value (mm/h).

The rain attenuation A_i (dB) suffered from the radio link i of rainy path length L can be estimated as [10]:

$$A_i = \int_0^L k_f R_i(l)^{\alpha_f} dl = \sum_{k=1}^N k_f R_i(k)^{\alpha_f} d_{pix} \quad (1)$$

where k_f and α_f are rain rate-to-specific attenuation conversion coefficients that depend on the hydrometeors properties (e.g. Drop Size Distribution, DSD, and temperature), on the link elevation angle, on the wave polarization, and, mainly, on the operational frequency. k_f and α_f can be derived from recommendation P.838-3 made available by the ITU-R (International Telecommunication Union – Radio communication sector) [13]: as an example, considering a vertically polarized wave and a link with elevation angle $\theta = 37^\circ$, k_f and α_f are comprised in the interval

0.0115–0.6495 and 1.2236–0.791, respectively, for frequencies in the range 10–50 GHz.

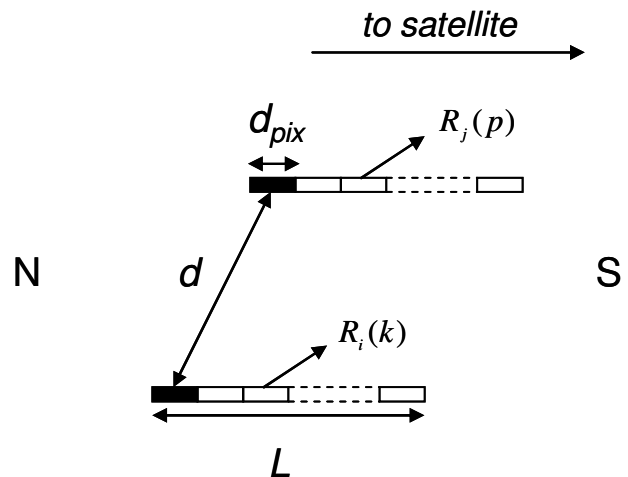


Fig. 1. Reference geometry depicting two parallel radio links with the same path length L affected by rain.

The objective of this work is to define an analytical formulation to express the spatial correlation of the attenuation impairing the two links as a function of the spatial correlation of the local point rain rate, as well as of the site separation distance d and of the link characteristics (geometrical and electrical). The spatial correlation of the attenuation and of the rain rate can be quantified by means of the correlation index [11],

$$\rho_A(A_i, A_j) = \frac{\text{cov}(A_i, A_j)}{\sigma[A_i] \sigma[A_j]} \quad (2)$$

and

$$\rho_R(R_i(k), R_j(p)) = \frac{\text{cov}(R_i(k), R_j(p))}{\sigma[R_i(k)] \sigma[R_j(p)]} \quad (3)$$

where $E[\bullet]$, $\sigma[\bullet]$ and $\text{cov}(\bullet, \bullet)$ are the mean, standard deviation and covariance operators, respectively. In the equations above, A_i and A_j are the attenuation time series, respectively relative to link i and link j , whilst $R_i(k)$ and $R_j(p)$ are the rain rate time series, respectively relative to pixel k of link i and pixel p of link j (refer to Fig. 1).

As an intermediate step towards the definition of the relationship between ρ_R and ρ_A , we first set $k_f = 1$ and $\alpha_f = 1$ in (1), i.e. we consider only the effect of integrating the rain rate along L by defining:

$$\bar{R}_i = \sum_{k=1}^N R_i(k) \quad \text{and} \quad \bar{R}_j = \sum_{p=1}^N R_j(p) \quad (4)$$

for link i and j , respectively. The spatial correlation index for the rain rate integrated along the rainy path is thus defined as:

$$\rho_r(\bar{R}_i, \bar{R}_j) = \frac{\text{cov}(\bar{R}_i, \bar{R}_j)}{\sigma[\bar{R}_i] \sigma[\bar{R}_j]} = \frac{\text{E}[\bar{R}_i \cdot \bar{R}_j] - \text{E}[\bar{R}_i] \text{E}[\bar{R}_j]}{\sigma[\bar{R}_i] \sigma[\bar{R}_j]} \quad (5)$$

According to the well-established quasi-ergodicity of the rainfall process [14],[15], long-term rain rate time series collected in different positions (e.g. by two raingauges) within the same area (as wide as approximately 200 km×200 km) tend to follow the same statistical distribution [16],[17]; therefore:

$$\begin{aligned} \text{E}[R_i(k)] &= \text{E}[R_j(p)] = \mu \\ \sigma[R_i(k)] &= \sigma[R_j(p)] = \sigma_r \end{aligned} \quad (6)$$

Focusing on the numerator of (5) and considering (6), we can write:

$$\text{E}[\bar{R}_i] = \text{E}\left[\sum_{k=1}^N R_i(k)\right] = N \text{E}[R_i(k)] = N\mu \quad (7)$$

which also holds for $\text{E}[\bar{R}_j]$, and,

$$\text{E}[\bar{R}_i \bar{R}_j] = \text{E}\left[\sum_{k=1}^N \sum_{p=1}^N R_i(k) R_j(p)\right] = \sum_{k=1}^N \sum_{p=1}^N \text{E}[R_i(k) R_j(p)] \quad (8)$$

Thus, the numerator in (5) can be written as:

$$\begin{aligned} \text{cov}(\bar{R}_i, \bar{R}_j) &= \sum_{k=1}^N \sum_{p=1}^N \{\text{E}[R_i(k) R_j(p)] - \mu^2\} = \\ &= \sum_{k=1}^N \sum_{p=1}^N \text{cov}(R_i(k), R_j(p)) \end{aligned} \quad (9)$$

and, by inverting (3), equation (9) becomes:

$$\text{cov}(\bar{R}_i, \bar{R}_j) = \sum_{k=1}^N \sum_{p=1}^N \rho_r(R_i(k), R_j(p)) \sigma_r^2 \quad (10)$$

Let us now take into account the denominator of (5):

$$\begin{aligned} \sigma[\bar{R}_i] &= \sqrt{\text{var}\left[\sum_{k=1}^N R_i(k)\right]} = \\ &= \sqrt{\sum_{k=1}^N \text{var}[R_i(k)] + 2 \sum_{k=1}^{N-1} \sum_{t=k+1}^N \text{cov}(R_i(k), R_i(t))} = \\ &= \sqrt{N \sigma_r^2 + 2 \sum_{k=1}^{N-1} \sum_{t=k+1}^N \rho_r(R_i(k), R_i(t)) \sigma_r^2} \end{aligned} \quad (11)$$

which also holds for $\sigma[\bar{R}_j]$.

As a result, based on (10) and (11), the spatial correlation index for the rain rate integrated along L can be expressed as follows:

$$\rho_r(\bar{R}_i, \bar{R}_j) = \frac{\sum_{k=1}^N \sum_{p=1}^N \rho_r(R_i(k), R_j(p))}{N + 2 \sum_{k=1}^{N-1} \sum_{t=k+1}^N \rho_r(R_i(k), R_i(t))} \quad (12)$$

The expression in (12) combines different values of the point rain rate correlation coefficient. Specifically, the

denominator takes into account the distance between points along the same link, whilst the numerator involves sites pertaining to the two different links. Under the hypothesis of spatial stationarity, which is a well-accepted concept for rain fields approximately as wide as 200 km×200 km [18], the rainfall correlation between two points is assumed to depend only on the distance between them and not on their positions within the field. Thus, the denominator of (12), W , can be simplified by the fact that pixels along the link separated by the same distance d will be associated to the same correlation value. As a result, with simple reasoning, W can be simplified as:

$$W = N + \sum_{n=1}^N (N - n + 1) \bar{\rho}_r(d_n) \quad (13)$$

where $\bar{\rho}_r(d_n)$ is the average value of $\rho_r(R_i(k), R_i(t))$ calculated on all the couples of pixels (belonging to the same link) at the same distance $d_n = n \cdot d_{pix}$.

The simplification of the numerator in (12), K , is more cumbersome because it involves the spatial correlation between all the pixels of links i and j . As sketched in Fig. 2 where the couple of pixels (k_3, p_8) is taken as a reference, the complexity arises from the fact that the distance d_{pk} depends not only on the relative position between the two stations (i.e. both on d and γ), but also on the relative positions of the two pixels in links i and j (i.e. on T).

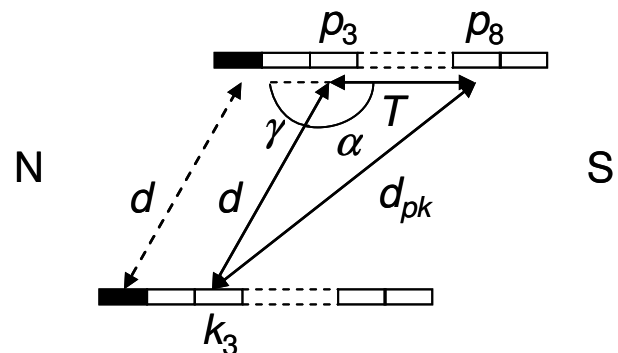


Fig. 2. Reference scheme for the calculation of \bar{d}_{pk} , the average distance between two pixels pertaining to two different links.

Making reference to Fig. 2, according to the Carnot's theorem, the distance d_{pk} can be written as:

$$d_{pk} = \sqrt{T^2 + d^2 - 2 d T \cos(\alpha)} = \sqrt{T^2 + d^2 + 2 d T \cos(\gamma)} \quad (14)$$

where $T = |p - k| d_{pix}$.

The average value of d_{pk} can be obtained by considering all the possible relative positions of two links for a fixed value of d . In mathematical terms:

$$\bar{d}_{pk} = \frac{1}{2\pi} \int_0^{2\pi} d_{pk} d\gamma = \frac{1}{2\pi} \int_0^{2\pi} \sqrt{T^2 + d^2 + 2 d T \cos(\gamma)} d\gamma \quad (15)$$

The closed-form solution of (15), whose details are given in Appendix A, yields:

$$\bar{d}_{pk} = \frac{2(T+d)}{\pi} E \left[\frac{4dT}{(T+d)^2} \right] \quad (16)$$

where $E(m)$ is the complete elliptic integral of the second kind (typically tabulated in numerical calculation software products, e.g. Matlab[®]), defined as:

$$E(m) = \int_0^{\pi/2} \sqrt{1 - m \sin^2(\theta)} d\theta \quad (17)$$

As an example, for $T = 4$ km and $d = 5$ km, equation (16) yields $\bar{d}_{pk} = 5.84$ km.

The last step to formulate ρ_A as a function of ρ_R requires to introduce in (12) the rain rate-to-specific attenuation conversion coefficients k_f and α_f . Based on equations (7) through (11), it can be easily shown that $\rho_A(A_i, A_j)$ will not depend on k_f and d_{pix} . Therefore:

$$\rho_A(A_i, A_j) = \frac{\sum_{k=1}^N \sum_{p=1}^N \rho_R(R_i(k)^{\alpha_f}, R_j(p)^{\alpha_f})}{N + 2 \sum_{k=1}^{N-1} \sum_{i=k+1}^N \rho_R(R_i(k)^{\alpha_f}, R_i(i)^{\alpha_f})} \quad (18)$$

If $\alpha_f = 1$, obviously $\rho_A(A_i, A_j) = \rho_R(\bar{R}_i, \bar{R}_j)$. If $\alpha_f \neq 1$, it is cumbersome, if even possible, to obtain an exact analytical relationship between ρ_A and ρ_R . However, the following approximation holds for $\alpha_f \approx 1$:

$$\rho_R(R_i(k)^{\alpha_f}, R_j(p)^{\alpha_f}) \approx [\rho_R(R_i(k), R_j(p))]^{\alpha_f} \quad (19)$$

Equation (19) has been derived by exploiting the Taylor expansion for the moments of functions of random variables [19], i.e. for the univariate and bivariate average and standard deviation of $R_i(k)^{\alpha_f}$ and $R_j(p)^{\alpha_f}$ involved in the calculation of the correlation coefficient in (19). As mentioned above, equation (19) is valid under the assumption that $\alpha_f \approx 1$ and therefore it is expected to be less and less accurate as α_f diverges more and more from 1. Although the approximation proposed in (19) may appear to be quite rough for some of the α_f values considered in this work (as mentioned in section II, $1.2236 \leq \alpha_f \leq 0.791$ for $10 \leq f \leq 50$ GHz), as it will be shown in the next section, its overall effect on ρ_A turns out to be very limited because the error inherent in the application of (19) tends to be cancelled out by the division in (18).

Based on (19) and under the hypothesis of spatial stationarity (already considered in the derivation of (13)) for which $\rho_R(R_i(k), R_j(p))$ can be replaced by $\bar{\rho}_R(\bar{d}_{pk})$, we thus obtain the final analytical expression for the average value of

the rain attenuation correlation index:

$$\bar{\rho}_A(d) \approx \frac{\sum_{k=1}^N \sum_{p=1}^N [\bar{\rho}_R(\bar{d}_{pk})]^{\alpha_f}}{N + \sum_{n=1}^N (N-n+1) [\bar{\rho}_R(d_n)]^{\alpha_f}} \quad (20)$$

$\bar{\rho}_A(d)$ depends on the distance between the transceivers d (included in \bar{d}_{pk}), on the rainy path through N and, finally, on the link wave polarization, frequency and elevation angle (included in α_f).

III. ACCURACY OF THE PROPOSED ANALYTICAL MODEL

In this section, rain field data derived from an extensive network of weather radars are used to evaluate the accuracy of the analytical expression presented in section II for the prediction of the rain attenuation decorrelation trend.

A. The weather radar database

The NIMROD network, managed by the UK Meteorological Office (MetOffice), consists of 19 C-band weather radars deployed across the British Isles. The position of the radar sites is indicated as asterisks in Fig. 3, which also depicts the overall coverage of the network.

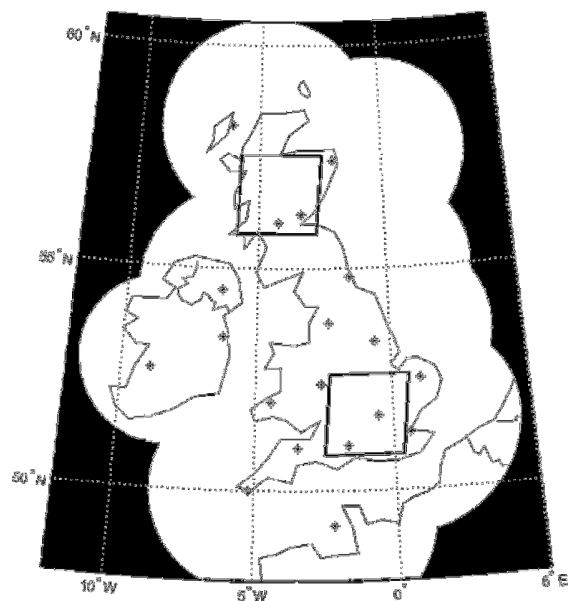


Fig. 3. Overall coverage of the NIMROD network and areas selected in this study (the asterisks indicate the radar sites).

Each radar performs in 5-minute time a series of azimuth scans at different elevations. Afterwards, the acquired data are centralized to Radarnet IV, the MetOffice processing system at Exeter, in full resolution polar format. All basic processing, quality controls and correction procedures, such as the elimination of ground clutter and the conversion of radar reflectivity Z (mm^6/m^3) into rain rate R (mm/h), are carried out on polar data [20]. The conversion of raw data to a Cartesian

grid is achieved by combining the various scans of multiple radars available at each pixel: the resulting composite rain maps represent a reliable estimate of the rain rate at ground level over the Great Britain, have 1 km×1 km grid spacing and are available every 5 minutes.

In this work, a full year (2009) of NIMROD 1 km×1 km composite rain maps, freely available on the web for research purposes [21], have been selected to assess the validity and the limitations of the analytical expression in (20). The whole database consists of 99695 maps, which corresponds to an availability of 94.84%.

B. Radar data processing

NIMROD composite images, whose size is 2175 km×1725 km, cover a large region characterized by different climatic features. As indicated by the black solid squares in Fig. 3, two areas have been selected, one in the North (coordinate of the square center: latitude = 56.66° N and longitude = -4.20° E) and one in the South (coordinate of the square center: latitude = 51.72° N and longitude = -0.94° E) with the aim of assessing whether, and to what extent, the accuracy of (20) depends on the local features of the rainfall process. The selected areas cover only the land, where the characterization of rain attenuation is of major interest for propagation-oriented applications, and have been limited to 200 km×200 km for the assumptions of quasi-ergodicity and spatial stationarity of the rain field to hold.

NIMROD maps have been processed to calculate the rain rate correlation index between all the couples of pixels included in each 200 km×200 km reference area using time series as input to (3). Results are shown in Fig. 4 for the Southern area, where the light gray dashed line represents the average value of the rain rate correlation index for a given site separation distance (referred to as $\bar{\rho}_R(d)$ in the previous section); the gray color scale in the background represents the density of the correlation index values, which provides a hint of the dispersion of ρ_R around $\bar{\rho}_R(d)$.

The rain rate correlation index steeply decreases for d values between 0 and 50 km and afterwards slowly tends to 0 for $d > 100$ km. Moreover the fairly limited dispersion of ρ_R represents an a-posteriori validation of the spatial stationarity of the rain field, which has been assumed in the derivation of (20). Fig. 5 reports the same results as in Fig. 4 but for the Northern area: with respect to the Southern area, a larger dispersion (average standard deviation of ρ_R over all distances equal to 0.03 and 0.05 for South and North, respectively) and a slower average decorrelation trend ($\bar{\rho}_R(25\text{km}) = 0.23$ and $\bar{\rho}_R(25\text{km}) = 0.34$ for South and North, respectively) emerge. The former indicates a more limited validity of the spatial stationarity of the rain field, probably associated with the presence of the Scottish Highlands (the opposite is true for the flat area in the South), whilst the latter is likely related to the prevalence of stratiform precipitation events affecting the Northern area (on the contrary, higher convective activity in the South), typically characterized by large spatial extent.

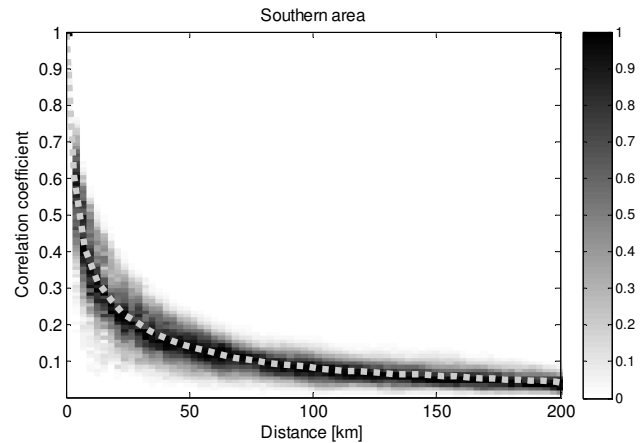


Fig. 4. Southern area: NIMROD derived average value of the rain rate correlation index ($\bar{\rho}_R(d)$, light gray dashed line) for a given site separation distance. Also depicted is the density of the rain attenuation correlation index (gray color scale in the background).

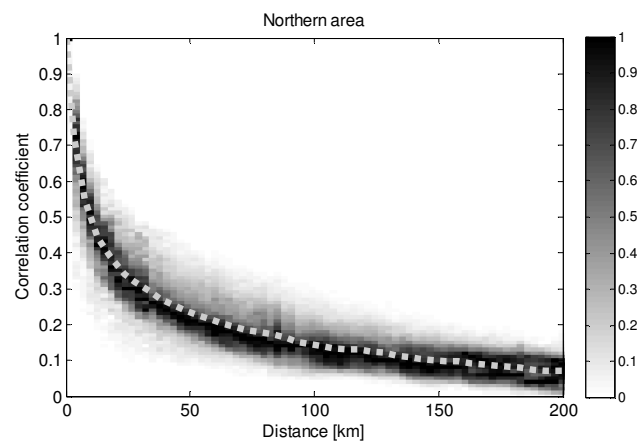


Fig. 5. Northern area: NIMROD derived average value of the rain rate correlation index ($\bar{\rho}_R(d)$, light gray dashed line) for a given site separation distance. Also depicted is the density of the rain attenuation correlation index (gray color scale in the background).

In order to assess the spatial correlation of the rain attenuation from NIMROD data, first radar maps have been converted into attenuation maps using (1) by considering all the relative positions between the radio link and the rain field, i.e. by placing the link transceiver on each pixel of the rain map. Afterwards, the same procedure used to calculate $\bar{\rho}_R(d)$ has been applied to calculate $\bar{\rho}_A(d)$, the average trend of the rain attenuation correlation index. As an example, results are shown in Fig. 6 (Southern area) for a radio link operating at $f = 40$ GHz with vertical polarization, North-South orientation, rain height $h_R = 3$ km and elevation angle $\theta = 37^\circ$ ($L = h_R/\sin(\theta) \approx 5$ km); the rain rate-to-specific attenuation conversion coefficients derived from recommendation ITU-R P.838-3 are $k_f = 0.4302$ and $\alpha_f = 0.8468$ [13]. Fig. 6 also includes $\bar{\rho}_R(d)$ for convenience: the comparison between the two curves allows to appreciate the increased spatial correlation of the attenuation (e.g. $\bar{\rho}_R(25\text{km}) = 0.23$ and $\bar{\rho}_A(25\text{km}) = 0.34$). Finally, the dispersion of the correlation

index for rain attenuation is comparable to the one reported in Fig. 4.

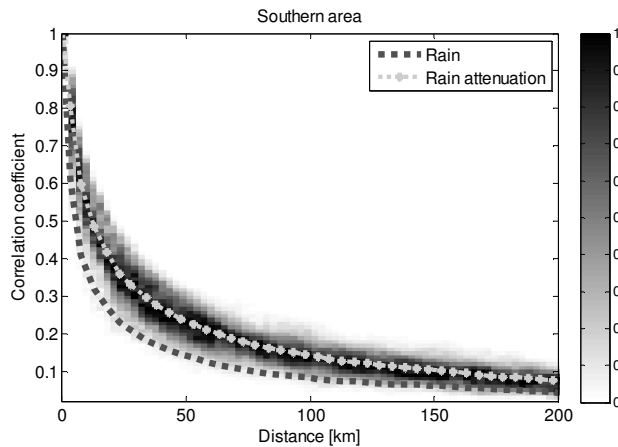


Fig. 6. Southern area: NIMROD derived average value of the rain rate ($\bar{\rho}_r(d)$, dark gray dashed line) and rain attenuation ($\bar{\rho}_A(d)$, light gray dotted line) correlation indexes for a given site separation distance. Also depicted is the density of the rain attenuation correlation index (gray color scale in the background).

Fig. 7 compares $\bar{\rho}_A(d)$ obtained from NIMROD data for different frequencies (same geometrical and electrical features of the links mentioned above).

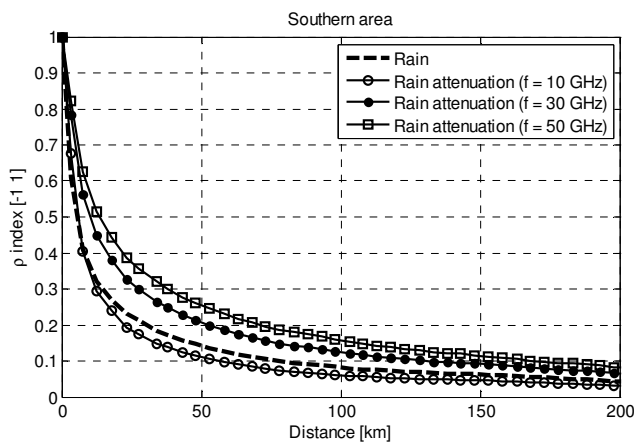


Fig. 7. Southern area: NIMROD derived average value of the rain attenuation correlation index for a given site separation distance: $f = 10, 30, 50$ GHz and rainy path length $L = 10$ km.

The figure points out that the marked increase in the spatial correlation of rain attenuation is not only due to the rain integration effect (see (1)), but also to the link frequency, such that, for example, $\bar{\rho}_A(25\text{km}) = 0.18, 0.32$ and 0.38 for $f = 10, 30$ and 50 GHz, respectively. This finding is related to the fact that, as elucidated by (20), $\bar{\rho}_A(d)$ depends on α_f and not on k_f ; while the specific attenuation $\gamma_A = k_f R^{\alpha_f}$ due to rain steeply increases with frequency (e.g. $R = 20$ mm/h yields $\gamma_A = 0.45, 3.63$ and 6.95 dB/km for $f = 10, 30$ and 50 GHz, respectively), α_f shows a decreasing trend with f ($\alpha_f = 1.2236, 0.9196$ and 0.791 for $f = 10, 30$ and 50 GHz, respectively). This finding

has an obvious consequence: at equal frequency, since α_f is associated with hydrometeor characteristics (i.e. mainly Drop Size Distributions and rain drop temperature), the rain attenuation decorrelation trend will also depend on the type of precipitation affecting the area of interest.

C. Assessment of the model's accuracy

The main inputs to estimate the spatial correlation of the rain attenuation by means of (20) are the rainy path length, L , and the average trend of the rain rate correlation index, $\bar{\rho}_r(d)$. Whilst the former can be determined from the knowledge of the geometrical and electrical characteristics of the link and of the local rain height (whose mean yearly value can be estimated for instance using recommendation ITU-R P.839-3 [22]), the latter can be derived from weather radar data (as shown in section III.B) or, alternatively, from networks of disdrometers and/or raingauges deployed in a given area [11],[23]. The application of (20) first requires to discretize L ; the choice of the most suitable value for d_{pix} is tightly linked to the spatial variability of rain: $d_{pix} = 1$ km is the suggested choice to guarantee a sufficient spatial sampling of the rain field and small N values (ranging between 5 and 8 for typical Earth-space links affected by rain) for a quick implementation of (20), but the choice of d_{pix} is obviously also dependent on the desired quantization precision for L (e.g. if $L = 4.5$ km, $d_{pix} = 0.5$ km may be a more suitable choice). Based on its derivation, equation (20) does not imply any lower bound for d , and, therefore, any limitation to the validity of the proposed model, which, in principle, is applicable also to micro scale site diversity configurations (distance between the links typically of the order of some hundreds of meters [23]). This would obviously require the knowledge of $\bar{\rho}_r(d)$ for distances equal or shorter than the desired d : based on the reference data available in this work, the assessment of the model's accuracy for distances smaller than the radar pixel lateral dimension (1 km for NIMROD data) is not possible.

As a final step, the calculation of $\bar{\rho}_A(d)$ by means of (20) requires resampling $\bar{\rho}_r(d)$ according to the different values of \bar{d}_{pk} and d_n included in the two summations. As an example, Fig. 8 shows the satisfactory estimation of $\bar{\rho}_A(d)$ achieved by applying (20).

The agreement between the two curves can be quantified by calculating the average ($E\epsilon$) and root mean square ($RMS\epsilon$) values of the following error figure:

$$\epsilon(d) = 100 \frac{\bar{\rho}_A(d)_{est} - \bar{\rho}_A(d)}{\bar{\rho}_A(d)} \quad (21)$$

where $\bar{\rho}_A(d)_{est}$ is the average value of the rain attenuation correlation index estimated through (20). For the example depicted in Fig. 8, as expected from the discussion on the approximation introduced in (19), the highest error is obtained for large separation distances ($10\% < \epsilon < 13\%$ for $d > 150$ km), whilst, overall, $E\epsilon = 3.2\%$ and $RMS\epsilon = 7\%$.

> REPLACE THIS LINE WITH YOUR PAPER IDENTIFICATION NUMBER (DOUBLE-CLICK HERE TO EDIT) <

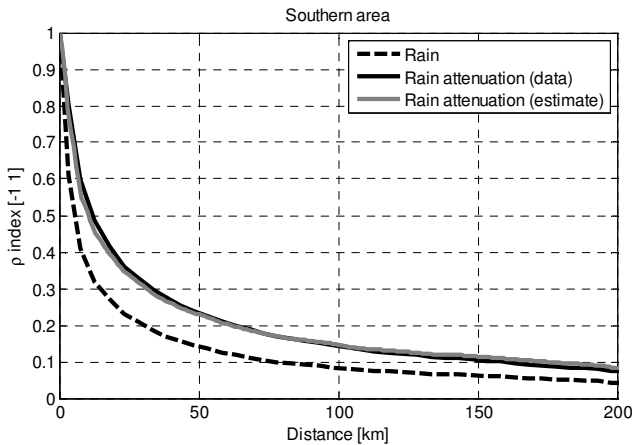


Fig. 8. Southern area: average value of the rain attenuation correlation index for a given site separation distance: $f = 40$ GHz, rainy path length $L = 5$ km. Comparison between curves derived from NIMROD data and estimate by means of (20).

Fig. 9 extends the assessment of the prediction accuracy delivered by (20) by depicting the results for the Southern area, in terms of $E\epsilon$ and $RMS\epsilon$, for different link frequencies and rainy path length $L = 5$ and 10 km. The latter represents an upper bound value of L for Earth-space links and has been introduced here to assess the impact of the rainy path length on the accuracy of analytical formulation of $\bar{\rho}_A(d)$ in (20).

The lowest and highest estimation errors are found for $f = 20$ GHz and $f = 50$ GHz, respectively, for both $L = 5$ km and $L = 10$ km. This behavior is tightly linked to the value of α_f , which, according to recommendation ITU-R P.838-3, is 0.9972 for $f \approx 20$ GHz and 0.791 for $f \approx 50$ GHz (vertical polarization and $\theta = 37^\circ$): as anticipated in the discussion on the approximation in (19), the error increases as α_f diverges from 1. On the other hand, Fig. 9 shows a limited impact of the estimation error on L . Finally, $E\epsilon$ indicates that, on the average, the estimation error is mainly associated to the overestimation of $\bar{\rho}_A(d)$ which, as mentioned for the results in Fig. 8, prevalently occurs for large site separation distances.

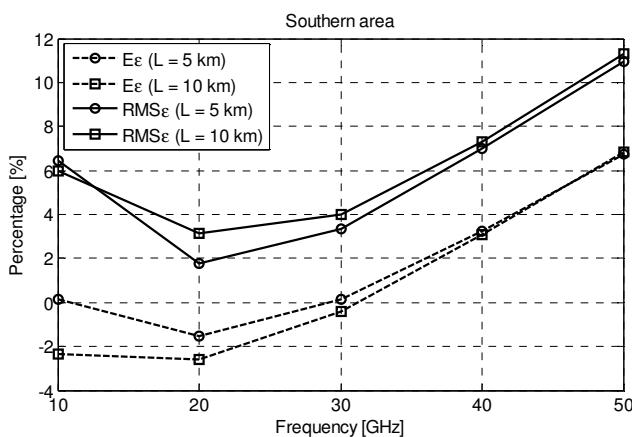


Fig. 9. Southern area: average ($E\epsilon$, dashed lines) and root mean square ($RMS\epsilon$, solid lines) values of the estimation error as a function of frequency for $L = 5$ km (circle markers) and $L = 10$ km (square markers). α_f values derived from recommendation ITU-R P.838-3.

Fig. 10 shows the same results as in Fig. 9, but for the Northern area. Again the lowest and highest errors are obtained for $f = 20$ GHz (or $f = 30$ GHz depending on L) and for $f = 50$ GHz, respectively. However, it is worth noting that the $RMS\epsilon$ is generally higher for the Northern area (e.g. considering $f = 50$ GHz and $L = 5$ km, $RMS\epsilon = 11\%$ and $RMS\epsilon = 18\%$ for South and North, respectively). This finding mainly depends on the fact that, in such area, the spatial stationarity assumption, inherently considered in the derivation of (20), is less acceptable than in the Southern area (refer to the scatter of ρ_R in Fig. 4 and Fig. 5).

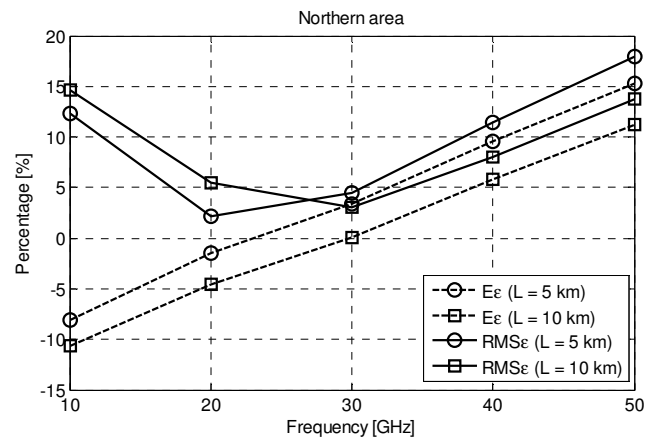


Fig. 10. Northern area: average ($E\epsilon$, dashed lines) and root mean square ($RMS\epsilon$, solid lines) values of the estimation error as a function of frequency for $L = 5$ km (circle markers) and $L = 10$ km (square markers). α_f values derived from recommendation ITU-R P.838-3.

In the light of the good prediction accuracy obtained, the proposed model represents a valuable tool for the accurate prediction of ρ_A from the local spatial correlation of the rain rate ρ_R , which, in turn, when not available from instruments such as weather radars and/or raingauges, could be derived according to [25] from rainfall data with coarse resolution included in global Numerical Weather Prediction (NWP) datasets (e.g. the ERA40 database [26]). The knowledge of ρ_A may reveal very useful for the improvement of the accuracy and flexibility of some propagation prediction models requiring information on the spatial correlation of rain attenuation. As an example, equation (20) could be beneficial for site diversity models such as [27] and [28], which estimate the joint rain attenuation distribution using a fixed expression for the decorrelation of rain attenuation with distance, whatever the rainy path length and carrier frequency. As an additional example of the applicability of (20), the knowledge of ρ_A could also improve the prediction of differential attenuation statistics between two Earth-space paths whose stations point to the same satellite [29], as well as the estimation of the interference statistical distribution in adjacent satellite networks [30].

The same mathematical framework presented in this paper can be quite easily extended to the case of converging links. Though this point is definitely worth being investigated, a

separate contribution would be needed to duly discuss the model's accuracy for converging links and its possible applications (e.g. orbital diversity for Earth-space paths or terrestrial links with various configurations and lengths).

IV. CONCLUSION

This contribution presents an analytical expression to predict the spatial correlation of the rain attenuation A impairing two Earth-space radio links in a site diversity configuration (ρ_A) as a function of the spatial correlation of the rain precipitation affecting the area (ρ_R). The estimated ρ_A also depends on the distance between the two stations d , the operational frequency f , the wave polarization and the rainy path length L . Well-established properties of the rain field (i.e. quasi-ergodicity and spatial stationarity) have been assumed in the derivation of the $\rho_A - \rho_R$ relationship, whose prediction accuracy was evaluated by exploiting an extensive set of rain field data collected by the NIMROD weather radar network in the UK. Specifically, tests focused on two 200 km×200 km regions of UK, one in the North and one in the South, with the aim of assessing the dependence of the prediction formula on the type of precipitation affecting the area of interest. Slightly worse prediction errors have been obtained in the North (hilly area, prevalently stratiform events), where the assumption of spatial stationarity was found to be less valid than in the South (flat area, both stratiform and convective events).

Negligible dependence of the prediction accuracy was found on the rainy path length L , whilst slightly higher errors were obtained for larger separation distances ($d > 150$ km). Moreover, as expected from the approximations introduced in deriving the prediction formula, the lowest prediction errors ($RMS\epsilon \approx 2\%$) were achieved for the frequency corresponding to $a_f \approx 1$ ($f \approx 20$ GHz for recommendations ITU-R P.838-3); on the contrary the highest errors ($RMS\epsilon \approx 18\%$) were obtained for frequencies associated to a_f most divergent from 1 (e.g. $f \approx 50$ GHz).

The analytical $\rho_A - \rho_R$ relationship derived in this work represents a useful and reliable tool to estimate from point rainfall data the decorrelation trend of rain attenuation, whose knowledge, in turn, is of key importance in the design of radio telecommunication systems taking advantage of the spatial inhomogeneity of rain to increase the overall performance of the system.

APPENDIX A

The average distance \bar{d}_{pk} is obtained as the solution of the following integral:

$$\begin{aligned} \bar{d}_{pk} &= \frac{1}{2\pi} \int_0^{2\pi} \sqrt{T^2 + d^2 + 2dT \cos(\gamma)} d\gamma \\ &= \frac{1}{\pi} \int_0^{\pi} \sqrt{T^2 + d^2 + 2dT \cos(\gamma)} d\gamma \end{aligned} \quad (A.1)$$

The simplification in the right-hand side of (A.1) is possible

because of the symmetricity of the geometry depicted in Fig. 2 with respect to the angle γ .

By applying the following substitution

$$\gamma = 2x \Rightarrow d\gamma = 2dx \quad (A.2)$$

we obtain:

$$\begin{aligned} \bar{d}_{pk} &= \frac{2}{\pi} \int_0^{\pi/2} \sqrt{T^2 + d^2 + 2dT \cos(2x)} dx \\ &= \frac{2}{\pi} \int_0^{\pi/2} \sqrt{T^2 + d^2 + 2dT[1 - 2\sin^2(x)]} d\gamma \end{aligned} \quad (A.3)$$

After few passages, equation (A.3) can be written as:

$$\begin{aligned} \bar{d}_{pk} &= \frac{2}{\pi} \int_0^{\pi/2} \sqrt{T^2 + d^2 + 2dT \left[1 - \frac{4dT}{T^2 + d^2 + 2dT} \sin^2(x) \right]} dx \\ &= \frac{2(T+d)}{\pi} \int_0^{\pi/2} \sqrt{1 - \frac{4dT}{(T+d)^2} \sin^2(x)} dx \end{aligned} \quad (A.4)$$

Naming $m = (4dT)/(T+d)^2$ and remembering that the complete elliptic integral of the second kind is defined as in (17), we finally obtain:

$$\bar{d}_{pk} = \frac{2(T+d)}{\pi} E \left[\frac{4dT}{(T+d)^2} \right] \quad (A.5)$$

ACKNOWLEDGMENT

The authors would like to thank the UK Meteorological Office and the British Atmospheric Data Center (BADC) for the elaboration and provision of NIMROD radar data, and Dr. Adrian Townsend from the University of Bath for kindly providing the software code to extract NIMROD 1 km×1 km composite images.

REFERENCES

- [1] <http://www.idirect.net/>. Accessed on May 2013.
- [2] L.J. Ippolito, "Effects of Precipitation on 15.3- and 31.65-GHz Earth-Space Transmissions With the ATS-V satellite", *Proceedings of the IEEE*, 59(2), 189-205, 1971.
- [3] R.K. Crane, F.E. Crane, "Electromagnetic Wave Propagation Through Rain", Wiley-Interscience, February, 1996.
- [4] B.C. Grémont, M. Filip, "Spatio-Temporal Rain Attenuation Model for Application to Fade Mitigation Techniques", *IEEE Transactions on Antennas and Propagation*, Vol. 52, No. 5, pp. 1245-1256, May 2004.
- [5] A. Paraboni, M. Buti, C. Capsoni, D. Ferraro, C. Riva, A. Martellucci, P. Gabellini, "Meteorology-Driven Optimum Control of a Multibeam Antenna in Satellite Telecommunications", *IEEE Transactions on Antennas and Propagation*, Vol. 57, No. 2, pp. 508-519, February, 2009.
- [6] J. Goldhirsh, B.H. Musiani, A.W. Dissanayake, L. Kuan-Ting, "Three-site space-diversity experiment at 20 GHz using ACTS in the Eastern United States", *Proceedings of IEEE*, 1997, 85:970-980.
- [7] S. Bertorelli, A. Paraboni, "Simulation of Joint Statistics of Rain Attenuation in Multiple Sites Across Wide Areas Using ITALSAT Data", *IEEE Transactions on Antennas and Propagation*, Vol. 53, No. 8, pp. 2611 - 2622, 2005.

> REPLACE THIS LINE WITH YOUR PAPER IDENTIFICATION NUMBER (DOUBLE-CLICK HERE TO EDIT) <

9

- [8] G. Karagiannis, A.D. Panagopoulos, J. Kanellopoulos, "Multi-Dimensional Rain Attenuation Stochastic Dynamic Modeling: Application to Earth-Space Diversity Systems", *IEEE Transactions on Antennas and Propagation*, vol. 60, no. 11, pp. 5400-5411, doi: 10.1109/TAP.2012.2208610.
- [9] A. Paraboni, C. Riva, C. Capsoni, G. Codispoti, L. Zuliani, V. Speziale, S. Falzini, A. Martellucci, E. Colzi, "Propagation and radar measurements performed in Spino d'Adda and the Italian planning for the Alphasat TDP5 scientific experiment", *European Conference on Antennas and Propagation (EuCAP)*, pp. 911-915, 23-27 March 2009.
- [10] L. Luini, N. Jeannin, C. Capsoni, A. Paraboni, C. Riva, L. Castanet, J. Lemorton, "Weather radar data for site diversity predictions and evaluation of the impact of rain field advection", *Int. J. Satell. Commun. Network*, 2011; 29:79-96. DOI: 10.1002/sat.953.
- [11] G.A. Baigorria, J.W. Jones, J.J. O'Brien, "Understanding rainfall spatial variability in southeast USA at different timescales", *Int. J. Climatol.*, 27: 749-760, 2007.
- [12] C. Capsoni, L. Luini, A. Paraboni, C. Riva, A. Martellucci, "A new prediction model of rain attenuation that separately accounts for stratiform and convective rain," *IEEE Transactions on Antennas and Propagation*, Vol 57, No. 1, pp. 196 - 204, 2009.
- [13] ITU-R P.838-3, "Specific attenuation model for rain for use in prediction methods", Propagation in non-ionized media, Geneva, 2005.
- [14] E.A.B. Eltahir, R.L. Bras, "Estimation of the fractional coverage of rainfall in climate models", *J. Climate*, Vol. 6, pp. 639-644, 1993.
- [15] C. Onof, H. Wheeler, "Analysis of the spatial coverage of British rainfall fields", *Journal of Hydrology*, 176 (1996), 97-113.
- [16] S. H. Lin, "A method for calculating rain attenuation distribution on microwave paths," *Bell Syst. Tech. J.*, vol. 54, no. 6, pp. 1051-1051, 1975.
- [17] K. Morita and I. Higuti, "Prediction methods for rain attenuation distributions of micro- and millimeter waves," *Rev. Electr. Commun. Lab.*, vol. 24, no. 7-8, pp. 651-668, Jul.-Aug. 1976.
- [18] T.L. Bell, "A space-time stochastic model of rainfall for satellite remote-sensing studies", *J. Geophysical Res.*, vol. 92, no. D8, pp. 9631-9643, Aug. 20, 1987.
- [19] J. Benjamin, A. Cornell, "Probability, Statistics and Decisions for Civil Engineering", McGraw-Hill, NY, 1970.
- [20] D.L. Harrison, S.J. Driscoll, M. Kitchen, "Improving precipitation estimates from weather radar using quality control and correction techniques", *The Meteorological Office*, Bracknell, Berkshire UK, October, 1998. Paper available online at <http://badc.nerc.ac.uk/browse/badc/ukmo-nimrod/doc/>.
- [21] NIMROD (2010), UK Meteorological Office. Rain radar Products (NIMROD). British Atmospheric Data Centre, 2003, August 2012. Data available at <http://badc.nerc.ac.uk/data/nimrod/>.
- [22] ITU-R P.839-3, "Rain height model for prediction methods", Propagation in non-ionized media, Geneva, 2001.
- [23] W.F. Krajewski, G. J. Ciach, J. R. McCollum, C. Bacotiu, "Initial validation of the Global Precipitation Climatology Project over the United States", *J. Appl. Meteor.*, 39, 1071-1086, 2000.
- [24] R.J. Acosta, E. Matricciani, C. Riva, "Slant Path Attenuation and Microscale Site Diversity Gain Measured and Predicted in Guam with the Synthetic Storm Technique At 20.7 GHz", *European Conference on Antennas and Propagation (EuCAP)*, pp. 1-4, 8-11 April 2013.
- [25] L. Luini, C. Capsoni, "The Impact of Space and Time Averaging on The Spatial Correlation of Rainfall", *Radio Sci.*, 47, RS3013, doi:10.1029/2011RS004915, 2012.
- [26] S.M. Uppala et al., "The ERA-40 Re-analysis", *Q. J. R. Meteorol. Soc.*, 131, 2961-3012, 2005.
- [27] ITU-R P.618-10, "Propagation data and prediction methods required for the design of Earth-space telecommunication systems", Propagation in non-ionized media, Geneva, 2009.
- [28] C.I. Kourogorgas, A.D. Panagopoulos, J.D. Kanellopoulos, "On the Earth-Space Site Diversity Modeling: A Novel Physical-Mathematical Outage Prediction Model", *IEEE Transactions on Antennas and Propagation*, vol. 60, no. 9, pp. 4391-4397, 2012.
- [29] ITU-R P.1815-1, "Differential rain attenuation", Propagation in non-ionized media, Geneva, 2009.
- [30] A.D. Panagopoulos, T.D. Kritikos, J.D. Kanellopoulos, "Adaptive Downlink Power Control Effects in Satellite Communication Networks: Interference Statistical Distribution", 13th Ka-Band Conference, Turin, September 2007.